

# Minimal energy packings and collapse of sticky tangent hard-sphere polymers

Robert S. Hoy and Corey S. O'Hern

*Department of Mechanical Engineering, Yale University, New Haven, CT 06520-8286 and  
Department of Physics, Yale University, New Haven, CT 06520-8120*

(Dated: August 13, 2010)

We enumerate all minimal energy packings (MEPs) for small single linear and ring polymers composed of spherical monomers with contact attractions and hard-core repulsions, and compare them to corresponding results for monomer packings. We define and identify “dividing surfaces” in polymer packings, which reduce the number of arrangements that satisfy hard-sphere and covalent bond constraints. Compared to monomer MEPs, polymer MEPs favor intermediate structural symmetry over high and low symmetries. We also examine the packing-preparation dependence for longer single chains using molecular dynamics simulations. For slow temperature quenches, chains form crystallites with close-packed cores. As quench rate increases, the core size decreases and the exterior becomes more disordered. By examining the contact number, we connect suppression of crystallization to the onset of isostaticity in disordered packings. These studies represent a significant step forward in our ability to predict how the structural and mechanical properties of compact polymers depend on collapse dynamics.

PACS numbers: 61.46.Bc, 64.70.km, 82.70.Dd, 64.60.Cn

Over the past several decades significant research activity has focused on understanding dense packings of hard spheres, since they serve as model systems for atomic and colloidal liquids and glasses, jammed granular media, and compressed foams and emulsions. An intriguing property of hard-sphere systems is that they can be prepared in crystalline, partially ordered, and amorphous packings [1]. Packings of ‘sticky’ hard spheres with contact attractions have been used to investigate self-assembly of colloidal particles with depletion attractions. Arkus *et al.* recently combined graph theory and geometrical techniques [2, 3] to enumerate minimal energy packings (MEPs), *i.e.* those with the maximum number of contacts, for  $N \leq 10$  sticky hard spheres. Their predictions agreed with experiments on attractive colloids [4].

However, there have been few studies of packings of sticky tangent hard-sphere *polymers*, which can model polymer collapse, protein folding, and protein interactions [5]. Recent simulations [6, 7] and experiments [8] have investigated polymer packings; however, they considered non-sticky spheres with only hard-core repulsions, where free volume, not energy, is relevant. Thus, there is little understanding of how covalent bond and chain uncrossability constraints affect structural and mechanical properties of sticky hard-sphere polymer packings and the probabilities with which these occur.

In this Letter, we perform exact enumeration studies of MEPs for sticky, tangent, monodisperse hard-sphere polymers (both linear and cyclic) and contrast the results with those for sticky hard spheres without polymer constraints. Our studies begin to address several overarching questions: 1) How do the probabilities for obtaining polymer MEPs differ from those for sticky hard-sphere MEPs? and 2) How do the properties of single compact polymers depend on collapse dynamics, *e.g.* do they collapse into crystalline or amorphous clusters?

Our results show that polymer constraints reduce the ways in which hard spheres can be arranged into MEPs, and the strength of this effect varies for different macrostates (*i.e.* structurally distinct packings). We demonstrate that the large reduction in the number of arrangements may be understood in terms of *dividing surfaces*. These split polymer packings into disjoint regions and eliminate particle-label permutations that do not correspond to polymer chains. We find that polymer MEPs with intermediate structural symmetry are more frequent relative to the monomer case, where entropy favors low symmetry MEPs [4].

In addition, using molecular dynamics (MD) simulations of temperature quenches at various rates  $\dot{T}$ , we show that single chains display glassy dynamics during collapse, and that the final polymer packings depend on  $\dot{T}$ . In the slow quench rate limit, the chains undergo a sharp [9] transition to crystallites, with a jump in the energy and number of contacts  $N_c$  (including covalent bonds) at temperature  $T = T_{\text{melt}}$ . The crystallites possess a close-packed core surrounded by a “surface” whose size and disorder increase with  $|\dot{T}|$ . For slow quenches,  $N_c$  at  $T_{\text{melt}}$  jumps from below the minimal number  $N_c^{\text{min}} = 3N - 6$  required for mechanical stability [10] to  $N_c^{\text{slow}}$ , where a significant fraction of the monomers possess 12 contacts. In the large  $|\dot{T}|$  limit, the clusters are disordered with  $\lesssim N_c^{\text{min}}$  contacts even as  $T \rightarrow 0$ , showing that rigidification can hinder crystallization.

We first describe exact enumeration methods for monomer and polymer MEPs [20]. To generate possible packings for a given number of spheres  $N$  and contact number  $N_c$ , we iterate over all  $N \times N$  adjacency matrices  $\bar{A}$  satisfying  $\sum_{j>i} A_{ij} = N_c$ . The elements of  $\bar{A}$  are 1 for contacting particles, and 0 for non-contacting particles and diagonal entries. Covalent bonds link sticky spheres to form a polymer chain with length  $N$ ;  $A_{i,i+1} = 1$  for

TABLE I: Statistics for MEPs with  $N$  spheres and  $N_c$  contacts.  $M$  is the number of macrostates,  $f_r$ ,  $f_p$ , and  $f_m$  are the fraction of microstates obeying minimal rigidity constraints that also satisfy hard-sphere constraints, respectively for rings, linear polymers, and monomers, and  $\Omega_r$ ,  $\Omega_p$ , and  $\Omega_m$  are the total numbers of microstates satisfying both minimal rigidity and hard-sphere constraints. Values for  $f$  and  $\Omega$  do not account for chiral twins [2]. In agreement with [2], we find 1 and 4 floppy macrostates (in the  $k \rightarrow \infty$  limit [20]), respectively for  $N = 9$  and ( $N = 10$ ,  $N_c = 24$ ). However, we find 2 and 55 more rigid macrostates<sup>\*,#</sup> for these cases [12, 20]. Adjacency matrices and coordinate solutions for all microstates are available online [21]. – indicates data not available.

$N$	$N_c$	$M$	$f_r$	$f_p$	$f_m$	$f_r/f_m$	$f_p/f_m$	$\Omega_r$	$\Omega_p$	$\Omega_m$
5	9	1	1	1	1	1	1	5	6	10
6	12	2	0.435	0.463	0.494	0.88	0.94	34	50	195
7	15	5	0.102	0.114	0.134	0.76	0.85	273	486	5712
8	18	13	$1.66 \cdot 10^{-2}$	$1.91 \cdot 10^{-2}$	$2.45 \cdot 10^{-2}$	0.68	0.78	2668	5500	231840
9	21	52 <sup>*</sup>	$1.40 \cdot 10^{-3}$	$2.46 \cdot 10^{-3}$	$3.34 \cdot 10^{-3}$	0.42	0.74	30663	71350	12368160
10	24	278 <sup>*,#</sup>	$2.21 \cdot 10^{-4}$	$2.55 \cdot 10^{-4}$	–	–	–	426590	1093101	–
10	25	3	$2.05 \cdot 10^{-6}$	$1.98 \cdot 10^{-6}$	–	–	–	5905	12138	–

$1 \leq i < N$  for linear chains, and additionally  $A_{1,N} = 1$  for rings. The distinction between permanent covalent and thermally fluctuating noncovalent bonds is not important for static packings; we include both types in  $N_c$ .

We enumerate all adjacency matrices satisfying the above conditions and then identify those that also fulfill hard-sphere and minimal rigidity constraints. Hard-sphere constraints imply that the center-to-center distances  $r_{ij}$  between unit spheres  $i$  and  $j$  obey  $r_{ij} \geq 1$ , where the equality holds for contacting pairs. Necessary conditions for rigidity are that each monomer possesses at least three contacts and  $N_c \geq N_c^{\min}$  [13].

To enforce these constraints, we implemented geometrical rules developed by Arkus *et al.* [2, 3] that eliminate invalid adjacency matrices. For the remaining configurations, we solved the system of quadratic equations

$$|\vec{r}_i - \vec{r}_j|^2 = d_{ij}^2 \quad (1)$$

for sphere positions  $\vec{r}_i$  to an accuracy of  $10^{-9}$ . We also calculated the dynamical matrix (all second derivatives of the energy in Eq. (2) with respect to monomer displacements) for all configurations, which allowed us to identify rigid (with  $3N - 6$  nonzero eigenvalues) and floppy configurations [13] (with fewer nonzero eigenvalues) [20].

From this procedure, we obtain microstates and macrostates for a given  $N$  and  $N_c$  that satisfy hard-sphere and minimal rigidity constraints and the relevant polymeric constraints. Each macrostate is characterized by an adjacency matrix that is nonisomorphic to and a set of interparticle distances  $\{r_{ij}\}$  that is different from those characterizing other macrostates [20]. With this definition, no macrostate can be rotated or reflected such that it yields a different macrostate. Every connected sticky hard-sphere macrostate admits a linear polymer macrostate [14]. Thus, sticky-sphere and linear polymer packings have identical macrostates. We have also verified this for ring packings for  $N \leq 10$ .

A microstate is a particular labeling of the particles 1 through  $N$  that comprise a  $N$ -particle macrostate with  $N_c$  contacts. Many microstates correspond to each macrostate due to particle permutations for monomer packings [4], and for polymers, the multiple possible paths through a given macrostate. The total number of microstates  $\Omega_m$ ,  $\Omega_p$ , and  $\Omega_r$  is given by the sum of microstates for each macrostate for monomers, linear polymers, and rings, respectively [20]. For monomer packings, which lack covalent bonds, the number of microstates for each macrostate (ignoring chirality) is given simply by a geometric factor  $\Omega_m^i = P_i$ , where  $P_i$  is the number of allowed permutations of particle indices for macrostate  $i$  [3]. For polymer packings, the number of microstates is not given by this relation since one must ensure that particle indices are consecutive.

Exact enumeration results are displayed in Table I, which shows the number of macrostates  $M$ , fraction  $f$  of adjacency matrices with  $N_c$  contacts obeying minimal rigidity that also satisfy hard-sphere constraints, and  $\Omega_m$ ,  $\Omega_p$ , and  $\Omega_r$  for  $5 \leq N \leq 10$ .  $f$  is the probability to obtain a packing for an ‘ideal’ protocol that samples adjacency matrices uniformly. From Table I, we see that  $f$  decreases approximately exponentially with  $N$  for  $N \geq 5$ , and even faster for  $N > 9$ . Part of the reason for the strong decrease in  $f$  between  $N = 9$  and 10 is the decrease in macrostates from 52 to 3. This occurs because  $N = 10$  MEPs possess  $N_c = N_c^{\min} + 1$ , which exceeds the number of degrees of freedom. Eq. 1 is then overconstrained, and its solutions possess special symmetries. The increase in  $N_c$  signals the onset of crystal nucleation, and the formation of a close-packed core. The ability to enumerate the numbers of isostatic ( $N_c = N_c^{\min}$ ) and hyperstatic ( $N_c > N_c^{\min}$ ) packings will yield insight into systems where glass and crystallization transitions compete.

For the  $N$  studied here, hard-sphere constraints are more difficult to satisfy for minimally rigid polymer packings compared to monomer packings:  $f_r < f_p < f_m$  [15].

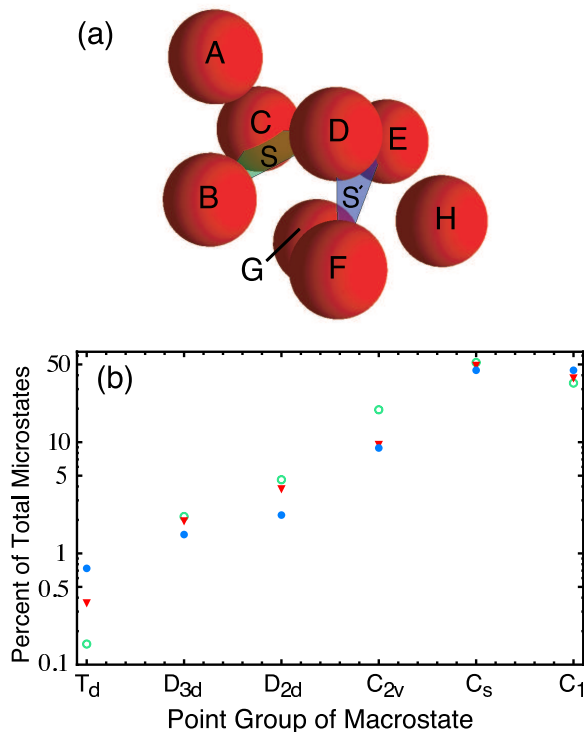


FIG. 1: (a) Schematic of dividing surfaces  $S$  and  $S'$  (colored triangles formed by monomers  $(B, C, D)$  and  $(D, E, F)$ , respectively) in a macrostate for  $N = 8$ . For  $S$ , region  $J$  consists of monomer  $A$  and region  $K$  of monomers  $(E, F, G, H)$ , or vice versa. (b) Fraction of microstates for packings from each symmetry group for cyclic (open circles) and linear (downward triangles) polymers, and monomers (filled circles) with  $N = 8$ . Results in (b) do not account for chiral structures.

A key mechanism for the reduction in  $f$  is the occurrence of “dividing surfaces” in polymer packings. A dividing surface is any minimal subset of a connected cluster of contacting monomers that geometrically splits it into two. Any polymer path that traverses a dividing surface that does not also topologically divide the polymer is blocked and invalid. Specifically, if  $m$  consecutive monomers  $i+1, \dots, i+m$  occupy an  $m$ -monomer dividing surface  $S$ , any polymer path where the sets of monomers  $J$  and  $K$  divided by  $S$  are anything other than  $1, 2, \dots, i$  and  $i+m+1, i+m+2, \dots, N$  (or vice versa) is blocked. In other words, any path that starts in  $J$ , enters  $S$ , and traverses it (passes through all monomers in  $S$ ) is blocked unless it traverses all monomers in  $J$  before entering  $S$ . Fig. 1(a) schematically depicts the sets  $J$  and  $K$  and two dividing surfaces for a  $N = 8$  macrostate. By definition, blocking does not occur in monomer packings.

In Table I, we see that the blocking effect increases sharply with  $N$  since  $f_r/f_m$  and  $f_p/f_m$  decrease significantly. Blocking also reduces [15] the fractions of allowed ring microstates relative to those for linear polymers  $f_r/f_p$  since rings do not possess chain ends. Another clear feature in Fig. 1(b) is that blocking changes the relative frequencies with which macrostates of differ-

ent symmetries are populated. Ring and linear polymer packings are more likely to possess intermediate symmetry than monomer packings, whereas the opposite is true for macrostates with the lowest and highest symmetries. Highly symmetric macrostates possess many distinct blocking surfaces, and low symmetry macrostates possess a surplus of closed trimers as shown in Fig. 1(a).

The enumeration studies illustrate an interesting competition between energy and entropy in large systems. For  $N \geq 10$ , MEPs are overconstrained with  $N_c > N_c^{\min}$ . This suggests that if the system becomes trapped in a metastable state (e.g. with  $N_c = N_c^{\min}$ ), rearrangements into MEPs will be slow because of their low entropy. Thus, glassy dynamics in single polymer chains should be observable in systems quenched at varying rates. For  $k_B T \gg |\epsilon|$ , where  $-\epsilon$  is the contact energy, polymers will adopt random-coil configurations with  $N_c \ll N_c^{\min}$ . As the polymer is cooled, one expects quench rate effects to become important when  $N_c \simeq N_c^{\min}$  [16].

To demonstrate glassy dynamics for single linear polymer chains, we employ MD simulations in which monomers interact via the potential energy

$$U_{\text{harm}}(r) = \begin{cases} -\epsilon + \frac{k}{2} \left( \frac{r}{D} - 1 \right)^2 & , \quad r < r_c \\ 0 & , \quad r > r_c \end{cases} \quad (2)$$

where  $k$  is the spring constant and  $D = 1$  is the monomer diameter. The temperature  $T$  is controlled via a Langevin thermostat. The unit of time is  $\tau = \sqrt{mD^2/\epsilon}$ , where  $m$  is the monomer mass. The cutoff radius  $r_c/D = \infty$  for covalently bonded monomers and  $1 + \sqrt{2\epsilon/k}$  for noncovalently bonded monomers.  $U_{\text{harm}}$  reduces to the energy for tangent sticky hard spheres [17] in the limit  $k \rightarrow \infty$  and possesses the same MEPs. For  $N \leq 10$ , the MEPs from simulations agree with those from complete enumeration for  $k \gtrsim 1600\epsilon$  ( $r_c \lesssim 1.04D$ ).

Figure 2(a) shows the potential energy per particle  $-U/N\epsilon$  for different quench rates  $\dot{T}$ . At low  $\dot{T}$ , a sharp transition between coils and crystallites [9, 11] is observed at  $T_{\text{melt}} \simeq 0.37\epsilon/k_B$ . The crystallites consist of a close-packed core with  $N_{cp}$  monomers (each with 12 contacts) and a less-ordered exterior. The crystallization transition corresponds (Fig. 2(b)) to a sharp transition in  $N_{cp}$ , which implies a change of symmetry within the core, from liquid-like to close-packed.

At higher rates, the dynamics becomes glassy near  $T_{\text{melt}}$ , and the systems do not approach the ground state energy even as  $T \rightarrow 0$ . We associate the suppression of crystallization with the onset of rigidity. Evidence for this is given in Fig. 2(c). The data show two “critical” quench rates:  $\dot{T}^*$  and  $\dot{T}^{**}$ . For  $|\dot{T}| < |\dot{T}^*|$ , the jump in  $N_c$  and  $N_{cp}$  resembles a first-order transition. For  $|\dot{T}| > |\dot{T}^{**}|$ , the systems do not form minimally rigid clusters even at  $T = 0$ . Even though the critical rates and  $T_{\text{melt}}$  are  $N$ -dependent, the trends are clear. For  $N = 100$  systems, we estimate  $|k_B \dot{T}^*/\epsilon| \sim 10^{-7}/\tau$  and  $|k_B \dot{T}^{**}/\epsilon| \sim 10^{-3}/\tau$ .

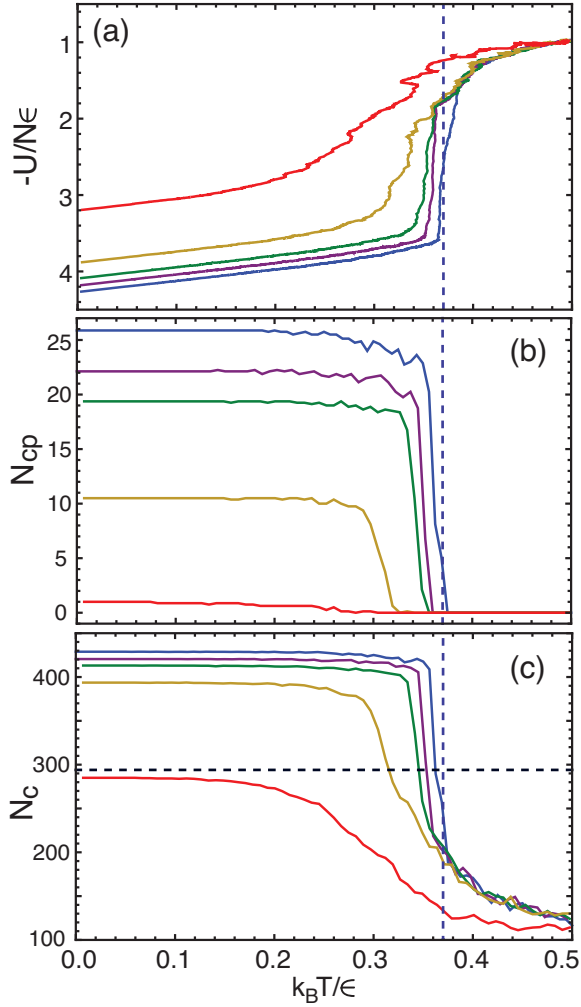


FIG. 2: (a) Potential energy per particle ( $-U/N\epsilon$ ) (b) number of particles with 12 contacts ( $N_{cp}$ ), and (c) total number of contacts ( $N_c$ ) versus  $k_B T/\epsilon$  for single linear polymers with  $N = 100$  at different quench rates. Data (top to bottom, panels b-c; bottom to top, panel a) are for quench rates  $k_B \dot{T}\tau/\epsilon = -10^{-3}, -10^{-4}, -10^{-5}, -10^{-6}$  and  $-10^{-7}$ . The critical quench rates are  $|k_B \dot{T}^*/\epsilon| \sim 10^{-7}/\tau$  and  $|k_B \dot{T}^{**}/\epsilon| \sim 10^{-3}/\tau$ . All results are averaged over several independent initial configurations. The horizontal (vertical) dotted lines indicate  $N_c = N_c^{\min}$  ( $k_B T/\epsilon = 0.37$ ).

The effects of quench rate on end states of quenches to  $T = 0$  are visualized in Fig. 3. Monomers are color-coded by the number of contacts; dark blue (red) indicates close packing ( $\ll 12$  contacts). The left panel shows a typical configuration after a fast quench with  $k_B \dot{T} = -10^{-4}\epsilon/\tau$ ; we see a small close-packed core surrounded by a disordered exterior. The middle and right panels show a collapsed structure at  $T = 0$  from a slow quench ( $k_B \dot{T} = -10^{-7}\epsilon/\tau$ ). The close-packed core is much larger, and the exterior is more crystalline. The large gaps visible in the rightmost panel indicate the order is hcp, and the structure is stack-faulted [18].

We examined minimal energy packings of sticky tangent hard-sphere linear and cyclic polymers, and com-

FIG. 3: Collapsed structures at  $T = 0$  for a single  $N = 100$  linear polymer using two quench rates:  $k_B \dot{T}\tau/\epsilon = -10^{-4}$  (left) and  $-10^{-7}$  (middle, right). The packing in the right panel is rotated compared to that in the middle panel to show its hexagonal planes.

pared them to monomer packings for small  $N$ . The packings are the same, but polymer packings possess significantly smaller entropies compared to monomer packings due to dividing surfaces, which arise from covalent-bond constraints. Entropic suppression via blocking is strongest for structures of both very high and low symmetry. In both monomer and polymer cases, the fraction of states satisfying hard-sphere constraints decreases at least exponentially with increasing  $N$ , and faster when  $N_c > N_c^{\min}$ . We also performed MD simulations of single linear chains with larger  $N$ , which link glassy dynamics to the onset of rigidity. This work sets the stage for future studies that investigate whether cooperative dynamics from chain connectivity and uncrossability constraints improves or impedes glass-forming ability of single polymers compared to colloidal systems.

We thank V. N. Manoharan for helpful discussions. Our results were obtained using the Boost Graph Library, a modified version of N. Arkus' structure solver [3], and LAMMPS [19]. Support from NSF Award No. DMR-0835742 and an Anderson Fellowship from Yale University is gratefully acknowledged.

## SUPPLEMENTARY MATERIAL FOR “MINIMAL ENERGY PACKINGS AND COLLAPSE OF STICKY TANGENT HARD-SPHERE POLYMERS”

In this supplementary material, we provide additional details concerning the methods employed to: (1) enumerate exactly all micro- and macrostates and (2) assess the rigidity for monomer and polymer packings composed of sticky, monodisperse tangent hard spheres.

### Exact enumeration method

The exact enumeration method consists of several steps including looping over all adjacency matrices satisfying the appropriate constraints for monomer and polymer packings, identifying those adjacency matrices that satisfy hard-sphere constraints, and then solving for their Euclidean positions.

The adjacency matrix  $\bar{A}$  for a  $N$ -particle system is a



$N \times N$  symmetric matrix whose elements are 1 for contacting particles and 0 for noncontacting particles. For monodisperse hard spheres,

$$\begin{aligned} A_{ij} &= 1 \text{ if } r_{ij} = D, \\ A_{ij} &= 0 \text{ if } r_{ij} > D, \end{aligned} \quad (3)$$

where  $r_{ij} = |\vec{r}_i - \vec{r}_j|$  is the center-to-center distance between spheres  $i$  and  $j$  and  $D$  is their diameter. By convention, the diagonal entries satisfy  $A_{ii} = 0$ .

The number of permutations for symmetric  $N \times N$  matrices with  $N_{\text{const}}$  constrained elements (*e.g.* covalent bonds) is

$$P_{\text{const}} = \frac{[(N^2 - N)/2]!}{N_{\text{const}}![(N^2 - N)/2 - N_{\text{const}}]!}, \quad (4)$$

where the  $(N^2 - N)/2$  terms arise because we only need to consider entries above the diagonal since  $\bar{A}$  is symmetric. The number of permutations  $P_{\text{cont}}$  for  $\bar{A}$  with  $N_c$  stickysphere contacts has the same form as Eq. 4:

$$P_{\text{cont}} = \frac{[(N^2 - N)/2]!}{N_c![(N^2 - N)/2 - N_c]!}. \quad (5)$$

For the packings considered in this study, the constrained elements correspond to covalent bonds, which are fixed to be 1 not 0. Thus, the number of permutations is

$$P_{\text{cct}}(N_{\text{const}}) = \frac{\left[\frac{N^2 - N}{2} - N_{\text{const}}\right]!}{(N_c - N_{\text{const}})! \left[\frac{N^2 - N}{2} - (N_c - N_{\text{const}})\right]!}, \quad (6)$$

where  $N_{\text{const}} = 0$ ,  $N - 1$ , and  $N$ , for monomers, linear polymers, and rings, respectively. Specifically, for linear and ring polymers,  $A_{i,i+1} = 1$  for  $1 \leq i < N$ . Rings must also satisfy the constraint  $A_{1,N} = 1$ . In contrast, monomer packings do not have explicitly constrained off-diagonal elements.

Thus, the numbers of adjacency matrices for monomers, linear polymers, and rings [22] for  $N$  particles and  $N_c$  contacts (including covalent bonds for polymers) are  $P_m = P_{\text{cont}}$ ,

$$\begin{aligned} P_{lp} &= P_{\text{cct}}(N - 1), \\ &= \frac{\left[\frac{N^2 - 3N + 2}{2}\right]!}{(N_c - (N - 1))! \left(\frac{N^2 - 3N + 2}{2} - (N_c - (N - 1))\right)!}, \end{aligned} \quad (7)$$

and

$$\begin{aligned} P_r &= P_{\text{cct}}(N), \\ &= \frac{\left[\frac{N^2 - 3N}{2}\right]!}{(N_c - N)! \left(\frac{N^2 - 3N}{2} - (N_c - N)\right)!}. \end{aligned} \quad (8)$$

We then loop through all permutations  $P_m$ ,  $P_{lp}$ , and  $P_r$  of  $\bar{A}$  for a given  $N$  and  $N_c$ . Since the entries of  $\bar{A}$

are ones and zeros, different adjacency matrices correspond to unique binary numbers (*i.e.* each microstate corresponds to a particular adjacency matrix and unique binary number). We enumerate all binary numbers using sequential binary permutations (from the C++ Standard Template Library *next\_permutation()* function). Note that considering polymers leads to an exponential reduction in the effort required for exact enumeration.

Since we are interested in minimal energy packings (MEPs)—those with the maximum number of contacts  $N_c$ , we focus on packings with  $N_c \geq N_c^{\text{min}}$ , where  $N_c^{\text{min}} \equiv 3N - 6$  is the minimal number of contacts required for rigidity. For  $4 \leq N \leq 9$ , we verified that no microstates with  $N_c > N_c^{\text{min}}$  satisfy hard sphere constraints (as shown previously [2]), and for  $N = 10$  no microstates with  $N_c = N_c^{\text{min}} + 2$  exist, *i.e.* MEPs for  $4 \leq N \leq 9$  possess  $N_c = N_c^{\text{min}}$  and for  $N = 10$  possess  $N_c = N_c^{\text{min}} + 1$ .

To eliminate adjacency matrices that do not satisfy hard-sphere constraints, we employed the complete set of geometrical rules for the adjacency matrices for  $N \leq 7$  provided in Ref. [3]. Specifically, we implemented rules 1-12, 14 – 18 outlined on pages 295-318. However, we did not employ the triangular bipyramid rule (discussed on pages 40-48 of [3]), neither the version for iterative packings nor that applied to new seeds. Instead, for  $N > 7$  we inserted those minimally rigid adjacency matrices not rejected by the geometrical rules into a modified version of Arkus' Euclidean structure solver. The structure solver makes a random initial guess for particle coordinates and then uses Newton's method to solve the contact equations implied by the adjacency matrix, while enforcing hard sphere constraints. We checked for convergence of the structure solver by increasing the maximum number of 'initial guesses' for the coordinates;  $3N^3$  initial guesses are sufficient to solve all structures to an accuracy in positions of  $10^{-6}$ .

Closely associated with  $\bar{A}$  is the distance matrix  $\bar{D}$  whose elements are  $D_{ij} = r_{ij}$ . For  $N < 10$  and  $N = 10$ ,  $N_c = 25$ , nonisomorphic  $\bar{A}$  (identified using the Boost Graph Library's *isomorphism()* function) correspond to different macrostates because the elements of  $\bar{D}$  are different [23]. However, for  $N = 10$ ,  $N_c = 24$  graph (non)isomorphism (as given by *isomorphism()*) is insufficient to completely distinguish macrostates. While there are 286 nonisomorphic graphs, 8 of these produce coordinate solutions that are identical to those produced by other graphs. All eight of these correspond to 'switching' a noncovalent bond in such a way that the same coordinate solution is produced. This reduces the total number of macrostates to 278.

For example, graphs 128 and 158 produce the same set of coordinates [21], but differ in that the former has a noncovalent bond between particles 1 and 6, while the latter possesses a noncovalent bond between particles 4 and 7. We assume that graphs 128 and 158 correspond to

the same macrostate because they possess the same  $\bar{D}$ , but (since the particles are distinguishable) the coordinate solutions correspond to different microstates [24]. We therefore have retained all microstates for all 286 graphs, but assign them to 278 macrostates. Adjacency matrices for graphs 128 and 158 and their common coordinate solution are shown below in (9); red entries indicate the ‘switched’ bond.

$$\begin{aligned}
 \text{Graph 128:} & \begin{bmatrix} 0 & 1 & 1 & 1 & 0 & \color{red}{1} & 1 & 1 & 1 & 1 \\ 1 & 0 & 1 & 0 & 1 & 1 & 0 & 0 & 0 & 1 \\ 1 & 1 & 0 & 1 & 1 & 0 & 0 & 0 & 1 & 1 \\ 1 & 0 & 1 & 0 & 1 & 1 & 0 & 1 & 0 & 0 \\ 0 & 1 & 1 & 1 & 0 & 1 & 0 & 0 & 0 & 0 \\ \color{red}{1} & 1 & 0 & 1 & 1 & 0 & 1 & 0 & 0 & 0 \\ 1 & 0 & 0 & 0 & 0 & 1 & 0 & 1 & 0 & 0 \\ 1 & 0 & 0 & 1 & 0 & 0 & 1 & 0 & 1 & 0 \\ 1 & 0 & 1 & 0 & 0 & 0 & 0 & 1 & 0 & 1 \\ 1 & 1 & 1 & 0 & 0 & 0 & 0 & 0 & 1 & 0 \end{bmatrix} \\
 \text{Graph 158:} & \begin{bmatrix} 0 & 1 & 1 & 1 & 0 & 0 & 1 & 1 & 1 & 1 \\ 1 & 0 & 1 & 0 & 1 & 1 & 0 & 0 & 0 & 1 \\ 1 & 1 & 0 & 1 & 1 & 0 & 0 & 0 & 1 & 1 \\ 1 & 0 & 1 & 0 & 1 & 1 & \color{red}{1} & 1 & 0 & 0 \\ 0 & 1 & 1 & 1 & 0 & 1 & 0 & 0 & 0 & 0 \\ 0 & 1 & 0 & 1 & 1 & 0 & 1 & 0 & 0 & 0 \\ 1 & 0 & 0 & \color{red}{1} & 0 & 1 & 0 & 1 & 0 & 0 \\ 1 & 0 & 0 & 1 & 0 & 0 & 1 & 0 & 1 & 0 \\ 1 & 0 & 1 & 0 & 0 & 0 & 0 & 1 & 0 & 1 \\ 1 & 1 & 1 & 0 & 0 & 0 & 0 & 0 & 1 & 0 \end{bmatrix} \\
 \text{Coordinates:} & \begin{bmatrix} 0 & 0 & 0 \\ 0 & 1 & 0 \\ -0.866025 & 0.5 & 0 \\ -0.57735 & 0 & -0.816497 \\ -0.57735 & 1 & -0.816497 \\ 0.288675 & 0.5 & -0.816497 \\ 0.288675 & -0.5 & -0.816497 \\ -0.481125 & -0.833333 & -0.272166 \\ -0.7698 & -0.333333 & 0.544331 \\ -0.288675 & 0.5 & 0.816497 \end{bmatrix}
 \end{aligned} \tag{9}$$

### Rigidity analysis

The rigidity of all macrostates generated by our exact enumeration algorithm was assessed by calculating the eigenvalues of the dynamical matrix [25], assuming the

following harmonic interparticle potential

$$U_{\text{harm}}(r) = -\epsilon + \frac{k}{2} \left( \frac{r}{D} - 1 \right)^2, \tag{10}$$

where  $D = 1$  and  $k$  must be large enough so that no ‘2nd-nearest neighbors’ interact. We have examined the number of rigid macrostates as a function of  $k$ . For sufficiently high precision in the coordinates (one part in  $10^6$  or better), all macrostates for  $4 \leq N \leq 8$  are rigid (*i.e.* the dynamical matrix possesses  $3N - 6$  positive eigenvalues) for  $k/\epsilon > 10$ . For the eigenvalue threshold, we assumed that eigenvalues  $e_i > 10^{-1}$  were nonzero and positive. For  $N = 9$ , we find one ‘floppy’ macrostate for all  $k/\epsilon > 400$ , consistent with Ref. [2]. We also verified that all  $N = 10$ ,  $N_c = 25$  macrostates possess are rigid.

For  $N = 10$ ,  $N_c = 24$ , however, the results show non-trivial dependence on the numerical precision of the coordinate solutions. When we solve for the coordinates to a precision of one part in  $10^9$ , we find 4 nonrigid (floppy) macrostates (in agreement with Ref. [2]) for all  $k/\epsilon > 400$ . However, when the coordinates are solved to a precision of only one part in  $10^6$ , one of the floppy configurations becomes ‘rigid’ in the same range of  $k$  due to insufficient precision.

Figure 4 shows the eigenvalue spectra for the  $N = 10$ ,  $N_c = 24$  macrostates for a precision of one part in  $10^9$  in the coordinate solutions. The eigenvalues are displayed from smallest to largest:  $j = 1$  to  $3N$ . The  $3N - 6$  positive eigenvalues for rigid macrostates are well-separated from the 6 eigenvalues that correspond to rigid translations and rotations as shown in panel (a). The eigenvalues corresponding to rigid translations and rotations (indexes 1-6) are zero to within our numerical precision. For floppy macrostates, the floppy eigenvalues are also orders of magnitude below those that correspond to finite-energy normal modes.

Since nonrigid macrostates have floppy modes that can be activated with no energy cost, each nonrigid macrostate possesses a continuum of coordinate solutions. However, we have verified that none of the four floppy macrostates for  $N = 10$ ,  $N_c = 24$  can be transformed continuously into one another (without increasing  $U_{\text{harm}}$ ). Specifically, we have shown that different coordinate solutions corresponding to the same floppy macrostate differ by  $\lesssim 10^{-3}D$ , while transitions between floppy macrostates would require displacements  $\sim D$ .

- 
- [1] C. S. O’Hern, L. E. Silbert, A. J. Liu, and S. R. Nagel, Phys. Rev. E **68**, 011306 (2003).
  - [2] N. Arkus, V. N. Manoharan, and M. P. Brenner, Phys. Rev. Lett. **103**, 118303 (2009).
  - [3] N. Arkus, Ph.D. thesis, Harvard University, 2009; <http://people.seas.harvard.edu/~narkus/assets/Thesis.pdf.zip>.

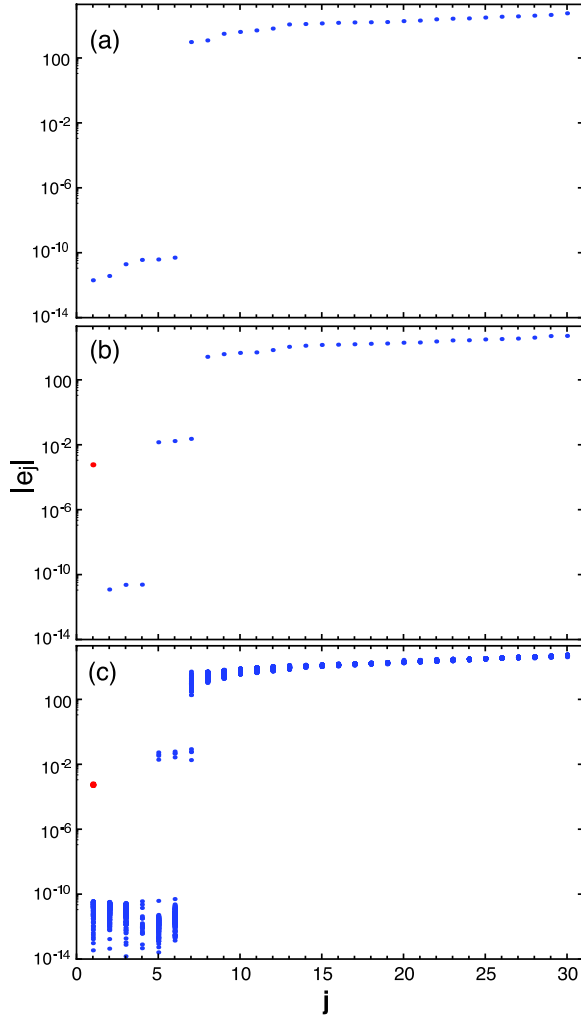


FIG. 4: Eigenvalue spectra from the dynamical matrix for  $N = 10$ ,  $N_c = 24$  macrostates. The eigenvalues  $e_j$  are sorted from smallest to largest,  $j = 1$  to  $3N$ . Eigenvalue spectra are shown for a rigid and floppy macrostate in (a) and (b) and all 278 macrostates in (c). In (a), there are  $3N - 6$  nonzero eigenvalues and 6 eigenvalues near zero that correspond to rigid translations and rotations. In (b), there is an extra ‘zero’ eigenvalue (red point) that corresponds to the floppy mode.

- [4] G. Meng, N. Arkus, M. P. Brenner, and V. N. Manoharan, *Science* **327**, 560 (2010).
- [5] T. T. Pham, M. Bajaj, and J. R. Prakash, *Soft Matter* **4**, 1196 (2008); M. J. Behe, E. E. Lattman, and G. D. Rose, *Proc. Natl. Acad. Sci.* **88**, 4195 (1991); L. Lo Conte, C. Chothia, and J. Janin, *J. Mol. Biol.* **285**, 2177 (1999).
- [6] M. Laso, N. C. Karayiannis, K. Foteinopoulou, M. L.

- Mansfield, and M. Kröger, *Soft Matter* **5**, 1762 (2009); N. C. Karayiannis, K. Foteinopoulou, and M. Laso, *Phys. Rev. E* **80**, 011307 (2009).
- [7] L. M. Lopatina, C. J. O. Reichhardt and C. Reichhardt, *cond-mat:0912.1874*.
- [8] L.-N. Zou et. al., *Science* **326**, 408 (2009).
- [9] It cannot be rigorously classified as first order since  $N = 100$  chains are far from the thermodynamic limit [11].
- [10] A. Donev, S. Torquato, and F. H. Stillinger, *Phys. Rev. E* **71**, 011105 (2005)
- [11] M. P. Taylor, W. Paul, and K. Binder; *J. Chem. Phys.* **131**, 114907 (2009), *Phys. Rev. E* **79**, 050801 (2009).
- [12] For  $N = 10$ ,  $N_c = 24$ , there are 279 macrostates; we list the 278 that cannot be formed by breaking one contact of a  $N = 10$ ,  $N_c = 25$  state [3].
- [13] D. J. Jacobs and M. F. Thorpe, *Phys. Rev. Lett.* **75**, 4051 (1995)
- [14] T. Biedl et. al., *Discrete Comput. Geom.* **26**, 269 (2001).
- [15] Except for ( $N = 10$ ,  $N_c = 25$ ); the slight difference may correspond to suppression of  $A$ ’s not satisfying minimal rigidity constraints.
- [16] A. Huerta and G. G. Naumis, *Phys. Rev. B* **66**, 184204 (2002).
- [17] S. B. Yuste and A. Santos, *Phys. Rev. E* **48**, 4599 (1993).
- [18] N. C. Karayiannis, K. Foteinopoulou, and M. Laso, *Phys. Rev. Lett.* **103**, 045703 (2009).
- [19] S. Plimpton, *J. Comp. Phys.* **117**, 1 (1995); <http://lammps.sandia.gov>
- [20] See the supplementary material for additional details of the exact enumeration methods and rigidity analyses.
- [21] The full set of adjacency matrices and coordinate solutions for all macrostates and microstates for monomer, linear polymer, and ring packings is available online at <http://ml313h.eng.yale.edu/~robhoy/MEPs.tar>.
- [22] Eqs. 4-8 break down in general if any of the arguments of the factorial terms become nonpositive.
- [23] Another factor that requires the macrostates to be defined with care is dimensionality. The Euclidean coordinate solutions are obtained by solving  $r_{ij}^2 = |\vec{r}_i - \vec{r}_j|^2 = d_{ij}^2$ . Some of the 278 ( $N = 10$ ,  $N_c = 24$ ) macrostates have the same sets of  $\{r_{ij}^2\}$  but different sets of  $\{r_{ij,x}^2, r_{ij,y}^2, r_{ij,z}^2\}$ ; this occurs because different sets of components  $r_{ij,x}^2$ ,  $r_{ij,y}^2$ , and  $r_{ij,z}^2$  (that do not correspond to rigid rotations) can give the same sum  $r_{ij}^2 = r_{ij,x}^2 + r_{ij,y}^2 + r_{ij,z}^2$ . This complication does not arise for  $N < 10$ , but we anticipate it will become increasingly important for enumeration of MEPs at higher  $N$ .
- [24] To see this, note that if the particles are distinguishable, we can assign ‘colors’ to them. Suppose 1 = “red”, 4 = “green”, 6 = “blue”, and 7 = “yellow”. Thus 128 contains a red-blue bond while 158 contains a green-yellow bond, and these are distinguishable at the microstate level.
- [25] G.-J. Gao, J. Blawdziewicz, and C. S. O’Hern, *Phys. Rev. E* **80**, 061303 (2009).